



NAVAL POSTGRADUATE SCHOOL

MONTEREY, CALIFORNIA

THESIS

**SIGNAL RECOVERY AND DETECTION OF CERTAIN
WIDEBAND SIGNALS USING MULTIPLE LOW-RATE
ADCs**

by

Michael A. Johnson

September 2018

Thesis Advisor:
Second Reader:

Ric Romero
David C. Jenn

Approved for public release. Distribution is unlimited.

THIS PAGE INTENTIONALLY LEFT BLANK

REPORT DOCUMENTATION PAGE			<i>Form Approved OMB No. 0704-0188</i>	
Public reporting burden for this collection of information is estimated to average 1 hour per response, including the time for reviewing instruction, searching existing data sources, gathering and maintaining the data needed, and completing and reviewing the collection of information. Send comments regarding this burden estimate or any other aspect of this collection of information, including suggestions for reducing this burden, to Washington headquarters Services, Directorate for Information Operations and Reports, 1215 Jefferson Davis Highway, Suite 1204, Arlington, VA 22202-4302, and to the Office of Management and Budget, Paperwork Reduction Project (0704-0188) Washington, DC 20503.				
1. AGENCY USE ONLY (Leave blank)		2. REPORT DATE September 2018		3. REPORT TYPE AND DATES COVERED Master's thesis
4. TITLE AND SUBTITLE SIGNAL RECOVERY AND DETECTION OF CERTAIN WIDEBAND SIGNALS USING MULTIPLE LOW-RATE ADCs			5. FUNDING NUMBERS RE239	
6. AUTHOR(S) Michael A. Johnson				
7. PERFORMING ORGANIZATION NAME(S) AND ADDRESS(ES) Naval Postgraduate School Monterey, CA 93943-5000			8. PERFORMING ORGANIZATION REPORT NUMBER	
9. SPONSORING / MONITORING AGENCY NAME(S) AND ADDRESS(ES) N/A			10. SPONSORING / MONITORING AGENCY REPORT NUMBER	
11. SUPPLEMENTARY NOTES The views expressed in this thesis are those of the author and do not reflect the official policy or position of the Department of Defense or the U.S. Government.				
12a. DISTRIBUTION / AVAILABILITY STATEMENT Approved for public release. Distribution is unlimited.			12b. DISTRIBUTION CODE A	
13. ABSTRACT (maximum 200 words) <p>There are certain wideband signals that occupy quite large bandwidths but may have dominant amplitudes in certain frequency bands. In this work, we show that these signals can be effectively sampled by a lower sampling rate compared to what is required by the Nyquist-Shannon sampling theorem. These resonant frequency components are split into separate receiver paths (subchains or channels) and sampled at a much lower sampling rate than is required for the entire wideband signal. It is shown that reconstruction of the signal is improved, and the probability of detection performance experiences little or no degradation since the effective noise power is attenuated by the proposed method.</p>				
14. SUBJECT TERMS Sub-Nyquist sampling, aliasing receiver, low-rate sampling, compressive sensing, wideband			15. NUMBER OF PAGES 53	
			16. PRICE CODE	
17. SECURITY CLASSIFICATION OF REPORT Unclassified	18. SECURITY CLASSIFICATION OF THIS PAGE Unclassified	19. SECURITY CLASSIFICATION OF ABSTRACT Unclassified	20. LIMITATION OF ABSTRACT UU	

THIS PAGE INTENTIONALLY LEFT BLANK

Approved for public release. Distribution is unlimited.

**SIGNAL RECOVERY AND DETECTION OF CERTAIN WIDEBAND SIGNALS
USING MULTIPLE LOW-RATE ADCs**

Michael A. Johnson
Lieutenant, United States Navy
BSME, University of Illinois at Urbana-Champaign, 2009

Submitted in partial fulfillment of the
requirements for the degree of

MASTER OF SCIENCE IN ELECTRICAL ENGINEERING

from the

**NAVAL POSTGRADUATE SCHOOL
September 2018**

Approved by: Ric Romero
Advisor

David C. Jenn
Second Reader

R. Clark Robertson
Chair, Department of Electrical and Computer Engineering

THIS PAGE INTENTIONALLY LEFT BLANK

ABSTRACT

There are certain wideband signals that occupy quite large bandwidths but may have dominant amplitudes in certain frequency bands. In this work, we show that these signals can be effectively sampled by a lower sampling rate compared to what is required by the Nyquist-Shannon sampling theorem. These resonant frequency components are split into separate receiver paths (subchains or channels) and sampled at a much lower sampling rate than is required for the entire wideband signal. It is shown that reconstruction of the signal is improved, and the probability of detection performance experiences little or no degradation since the effective noise power is attenuated by the proposed method.

THIS PAGE INTENTIONALLY LEFT BLANK

Table of Contents

1	Introduction	1
1.1	Previous Receiver Design Strategies	1
1.2	Our Approach	1
1.3	Objective	2
1.4	Thesis Organization	2
2	Signal Modeling	3
2.1	Modeling Wideband Signals of Interest	3
2.2	Example Signal	3
2.3	Multiple Low-Rate Sampler System Architecture.	6
3	Recovery and Detection Theory	9
3.1	Signal Recovery Error	9
3.2	Matched Filters	9
3.3	Probability of Detection — Matched Filter	10
3.4	Probability of Detection — MLRS	11
3.5	Monte Carlo Simulation	11
3.6	Recovered Signal	13
4	Test Signal Results	17
4.1	Simulation Configuration Parameters	17
4.2	Sum-Squared Error	17
4.3	Probability of Detection Results	19
4.4	Hardware Modeling	21
4.5	Hardware Results	22
5	Practical Target Model and Results	25
5.1	RCS Target Response.	25
5.2	Simulation Configuration Parameters	25

5.3	Sum-Squared Error	27
5.4	Probability of Detection.	27
6	Conclusion	31
6.1	Summary of Results	31
6.2	Future Work	31
	List of References	33
	Initial Distribution List	35

List of Figures

Figure 2.1	Wideband Signal Spectrum with Dominant Frequency Bands (top) and Subbands (bottom)	4
Figure 2.2	Test Signal Spectrum (top), Test Signal Spectrum with a Noise Realization (middle), and Time-Domain Test Signal (bottom)	5
Figure 2.3	Multiple Low-Rate Samplers (MLRS) Receiver	7
Figure 3.1	Test Signal in Noise Spectrum (top) and its Corresponding Reconstruction Spectrum (bottom)	10
Figure 3.2	Theoretical Matched Filter Detection Performance for a $P_{FA} = 10^{-2}$	12
Figure 3.3	Signal Detection Flowpath	13
Figure 3.4	Noise-Free Test Signal and its MLRS Reconstruction	14
Figure 3.5	White Gaussian Noise Spectrum (top) and its MLRS Reconstruction Spectrum (bottom)	15
Figure 4.1	MLRS and Traditional High-Rate Sampler Sum-Squared Error for Test Signal	18
Figure 4.2	MLRS and Matched Filter Detection Performance for Test Signal for $P_{FA} = 10^{-2}, 10^{-3}$, and 10^{-4}	20
Figure 4.3	Simulink Receiver Subchain Model	22
Figure 4.4	Xilinx Zynq-7000 SoC ZC706	23
Figure 4.5	MLRS Hardware Detection Performance for Test Signal for $P_{FA} = 10^{-2}$	24
Figure 5.1	A6 Tank Model and Frequency Response for $\phi = 0^\circ$ and $\theta = 45^\circ$. Adapted from [11].	26
Figure 5.2	MLRS and Traditional High-Rate Sampler Sum-Squared Error for A6 Target Response	28

Figure 5.3 MLRS and Matched Filter Detection Performance (top) and MLRS
Hardware Detection Performance (bottom) for A6 Target Response 29

List of Tables

Table 4.1	Model Design Parameters for Test Signal	17
Table 5.1	Model Design Parameters for A6 Signal	26

THIS PAGE INTENTIONALLY LEFT BLANK

List of Acronyms and Abbreviations

ADC	analog-to-digital converter
BPF	bandpass filter
DFT	discrete frequency transform
FIR	finite-impulse response
FFT	fast Fourier transform
FPGA	field-programmable gate array
HDL	hardware description language
IC	integrated chip
I/Q	in-phase and quadrature
IF	intermediate frequency
LPF	lowpass filter
MC	Monte Carlo
MF	matched filter
MLRS	multiple low-rate samplers
RF	radio frequency
SD	secure digital
SNR	signal-to-noise ratio
SSE	sum-squared error
WGN	white Gaussian noise

THIS PAGE INTENTIONALLY LEFT BLANK

Acknowledgments

I would like to thank my wife and daughter for their support and patience. Professor Romero, thank you for the motivation and direction of this thesis.

THIS PAGE INTENTIONALLY LEFT BLANK

CHAPTER 1:

Introduction

The focus of the work presented here is to develop an innovative approach to receiver design for wideband signals with resonant frequency components. In hindsight, the proposed design is very intuitive, but the results and applications are profound. While many engineering solutions are driven towards all-encompassing answers, the method developed here is specialized to a specific class of signals. The lack of research and published work signifies the need for research in this area.

1.1 Previous Receiver Design Strategies

While the sampling theorem only requires slightly more than the Nyquist rate for detection, estimation, or reconstruction of bandlimited signals, in practice higher rates are actually used due to various radio frequency (RF) receiver effects such as signal distortion and noise. Thus, signals that have very large bandwidths require a very high-rate analog-to-digital converter (ADC), which may be costly or technologically impractical. Many studies have addressed the large bandwidth (in frequency) but sparse (in time) type of signals. Previous methods demonstrated by [1]–[3] use compressed sensing techniques, which rely on a sparse signal (in some domain) such that a very low sampling rate is feasible. For reconstruction, however, the computational burden and latency may be significant due to the optimization methods needed for signal reconstruction. Other methods [4] purposefully alias the signal and apply innovative filters to reconstruct the signal or apply polyphase filter banks to separate the signal [5].

1.2 Our Approach

Although some wideband signals may be sparse in the time domain due to the well-known frequency-time duality, in this work we are interested in large-bandwidth signals that are not necessarily sparse in the time domain. In other words, we investigate signals for which compressive sensing techniques may fail. Yet we still desire a receiver architecture which lowers the effective sampling rate needed for these types of signals. We propose a receiver capable of doing so in this work. Our proposed method also lowers the computational

burden. With our approach there is no need to alias the signal or apply a filter bank across the entire bandwidth of the signal as others have done. The signal processing architecture we propose is simple in nature, and the probability of detection performance is not degraded with the effective lower sampling rate. This approach is ideal for a programmable application specific receiver detecting a known signal of interest that is large in bandwidth and contains dominant frequency bands. We call our method the “multiple low-rate samplers” (MLRS) technique.

1.3 Objective

The technology described above is investigated using two performance metrics. First the sum-squared error (SSE) is determined to measure the similarity between the signal and its recovery or reconstruction. The MLRS is compared against a traditional high-rate sampling receiver. Next, we investigate probability of detection performance of the MLRS compared to the matched filter receiver. These results are generated via Matlab simulation, Simulink hardware simulation, and finally a field-programmable gate array (FPGA) implementation. A hypothetical signal and practical signal are modeled through the entire simulation process.

1.4 Thesis Organization

This thesis is organized into six chapters. Following the introduction in Chapter 1, the signal modeling and the MLRS system architecture are described in Chapter 2. The underlying theory for sum-squared error, probability of detection, matched filter design, and a general discussion on the signal processing in the MLRS receiver is outlined in Chapter 3. The results for the test signal along with a discussion on the FPGA hardware modeling and simulation are presented in Chapter 4. A practical signal is modeled and its results are given in Chapter 5. Finally, the conclusion and recommendations are summarized in Chapter 6.

CHAPTER 2: Signal Modeling

2.1 Modeling Wideband Signals of Interest

It is generally known that a carrier or passband signal can be downconverted to a complex baseband representation. Let $x(t)$ be a wideband, passband signal. Let $X(f)$ be the Fourier transform of $x(t)$. We consider $X(f)$ that contain dominant bands in the frequency domain such as the signal shown in the top panel of Figure 2.1. Since $X(f)$ has dominant bands, it can be approximated as the summation of the m prevailing frequency bands:

$$X(f) \approx \sum_{i=1}^m \psi_i(f), \quad (2.1)$$

where $\psi_i(f)$ is the i_{th} portion of the signal surrounding a given i_{th} carrier or center frequency f_i . The approximate representation is shown in the bottom panel of Figure 2.1. Let B_W be the bandwidth of the signal $X(f)$ and B_i be the bandwidth of the $\psi_i(f)$. It stands to reason the $\sum_{i=1}^m B_i \leq B_W$.

The received signal in the receiver is $s(t) = x(t) + w(t)$ where $w(t)$ is zero-mean white Gaussian noise. Traditionally, the received signal $s(t)$ requires sampling at greater than $2B_W$ according to Nyquist, but by partitioning the signal into m sections in the frequency domain, the signal $\psi_i(t)$ in each receiver subchain has a Nyquist rate of $2B_i$. In other words, we can use a lower sampling rate in each receiver subchain and lower effective total sampling rate.

2.2 Example Signal

Of course, the continuous-time signal is sampled in modern receivers. For simulation purposes, we can normalize the sampling time to $T_s = 1$, such that the corresponding signals are given by $x[n]$, $w[n]$, and $s[n]$ where $n = 0, 1, 2, \dots, N-1$. After fast Fourier transform (FFT) operations, the corresponding discrete frequency transforms (DFT) are given by $X[f]$ and $S[f]$. The DFT $X[f]$ can be approximated by $X[f] \approx \sum_{i=1}^m \psi_i[f]$,

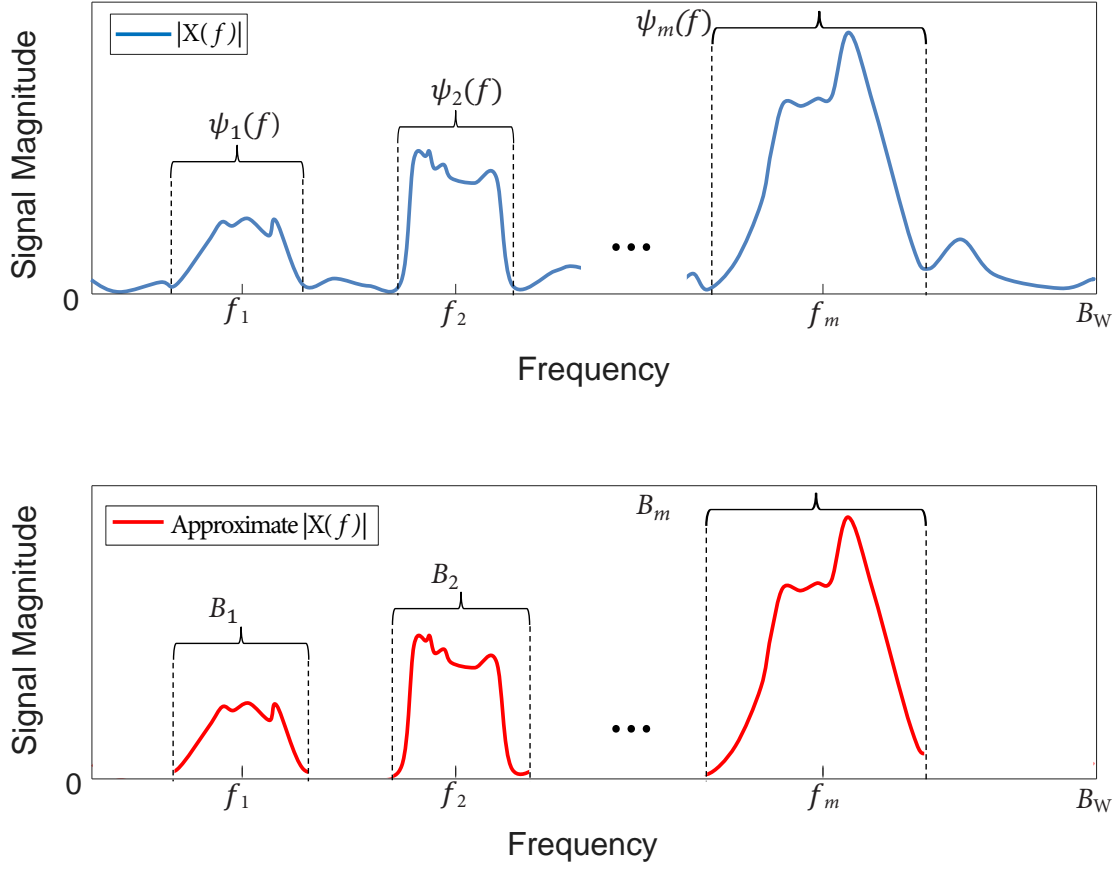


Figure 2.1. Wideband Signal Spectrum with Dominant Frequency Bands (top) and Subbands (bottom)

where $\psi_i[f]$ is the i_{th} portion of the discrete signal surrounding a given i_{th} carrier or center frequency. We also define \mathbf{x} , \mathbf{w} , and \mathbf{s} to represent the discrete time vectors for the sampled signals. We assume the noise \mathbf{w} to be white Gaussian noise.

Consider the signal $x[n]$ with the normalized magnitude spectrum $|X[f]|$ shown in the top panel of Figure 2.2. This signal is clearly wideband, with rich frequency content and dominant bands. Three prominent $\psi_i[f]$ are highlighted in the top panel. It is these three portions of the spectrum which are filtered into individual receiver subchains. In the middle panel, the magnitude spectrum of the received signal plus some noise realization is also shown. This signal is not sparse in the time domain as shown in the bottom panel of Figure 2.2.

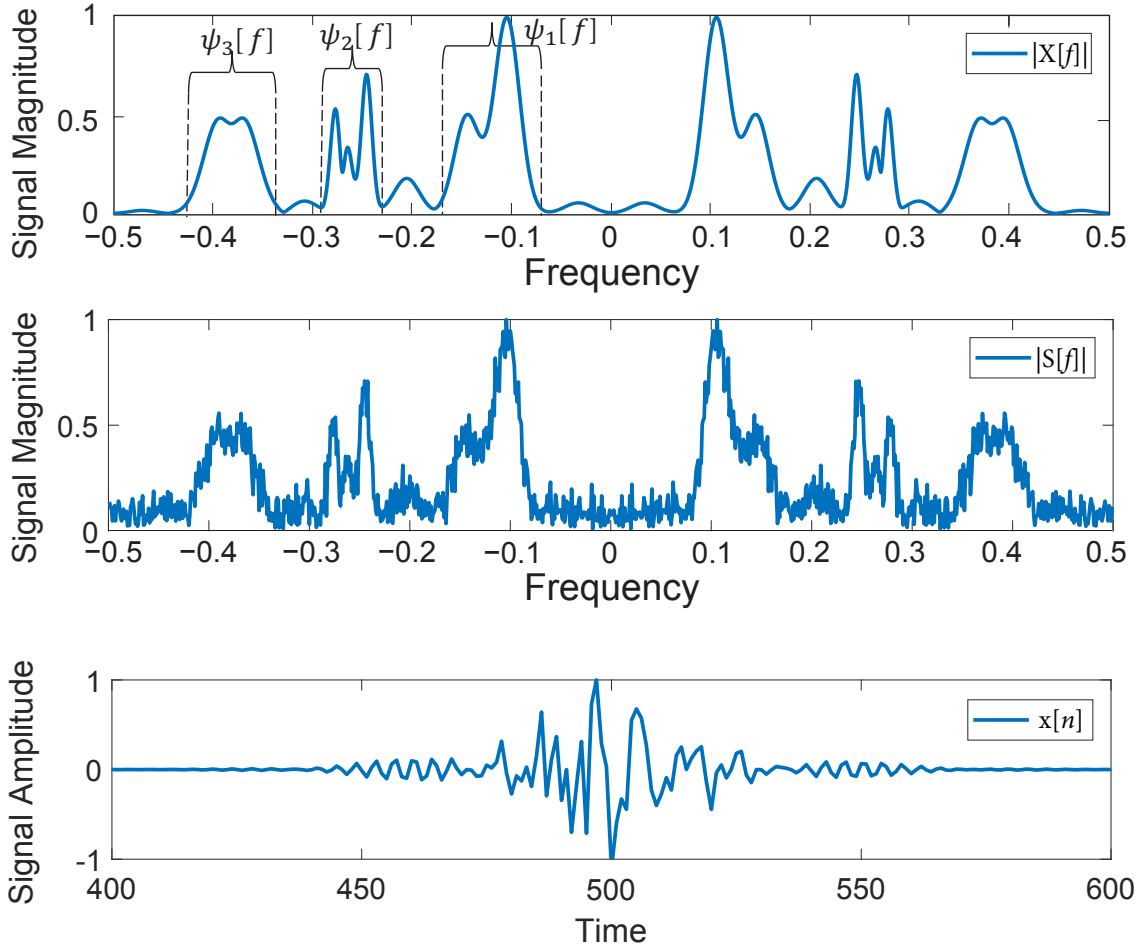


Figure 2.2. Test Signal Spectrum (top), Test Signal Spectrum with a Noise Realization (middle), and Time-Domain Test Signal (bottom)

2.2.1 Test Signal Creation

The arbitrary test signal $x[n]$ shown in Figure 2.2 was intentionally created to demonstrate a wideband signal which is not sparse in the time domain. This is necessary to demonstrate that the technique proposed here works successfully, while the other sub-Nyquist techniques previously mentioned do not. Although the signal is arbitrary, it is representative of actual signals. We begin in the frequency spectrum to generate the test time-domain signal. Signal shape and carrier frequencies are manipulated until the sought after response is achieved. The test signal is created to be magnitude-symmetric in the frequency domain to allow for both real and complex-valued signal possibilities. Obviously, the inverse Fourier transform ultimately converts the frequency domain signal into the desired time-domain waveform.

Note that each $\psi_i[f]$ has more than one local maximum across the selected bandwidth. In each receiver subchain, it is not necessary that the peak value be centered in the channel or that there exist only a single maximum. Multiple maxima can be grouped together and downconverted at a given center frequency.

2.3 Multiple Low-Rate Sampler System Architecture

In Figure 2.3 we show the proposed MLRS receiver. We already assume that the RF carrier is downconverted to an intermediate frequency (IF) signal $s(t)$. The IF signal is split (channelized) into m separate receiver subchains. Each subchain has a bandpass filter (BPF) centered at the IF frequencies f_1, f_2, \dots and f_m . Each BPF isolates each subband signal $\psi_i(f)$. Each subband signal is downconverted to baseband. The lowpass filter (LPF) in each subchain is a critical component since it acts to filter out the intermodulation products. Moreover, it acts as the antialiasing filter prior to analog-to-digital conversion. There are m low-rate ADCs whose effective total sampling rate is clearly lower than the entire signal's Nyquist rate. The entire signal's sampling rate F_s is given by $F_s \geq 2B_W$. Each subchain has a smaller bandwidth, thus a lower Nyquist rate. This lower rate is determined by comparing B_W to the B_i . This ratio is given by

$$D_i = \frac{B_W}{B_i}, \quad (2.2)$$

where D_i is the ratio of B_W to B_i in the i_{th} channel and is found by rounding down to the nearest integer value. The individual channel sampling frequency is given by

$$F_{s,i} \geq \frac{F_s}{D_i}, \quad (2.3)$$

where $F_{s,i}$ is the sampling frequency of the i_{th} channel.

Next, each subband signal corresponding to a subchain is fed into a digital architecture containing an FPGA/microprocessor module. Each subband signal is upconverted into its original IF center frequency. In other words, we assume that we can clock the digital module (the FPGA and the microprocessor) at a higher clock rate, i.e., higher than the clock rate for the low-rate ADCs. The subband signals are added for signal recovery.

For detection purposes, a matched filter is used. Since we completely know the MLRS receiver design and signal-of-interest $x[n]$, the actual MLRS matched filter is developed

from noise-free reconstruction $\tilde{x}[n]$. While the signals are very similar, the optimal filter for MLRS is based on the noise-free reconstruction and not the original signal.

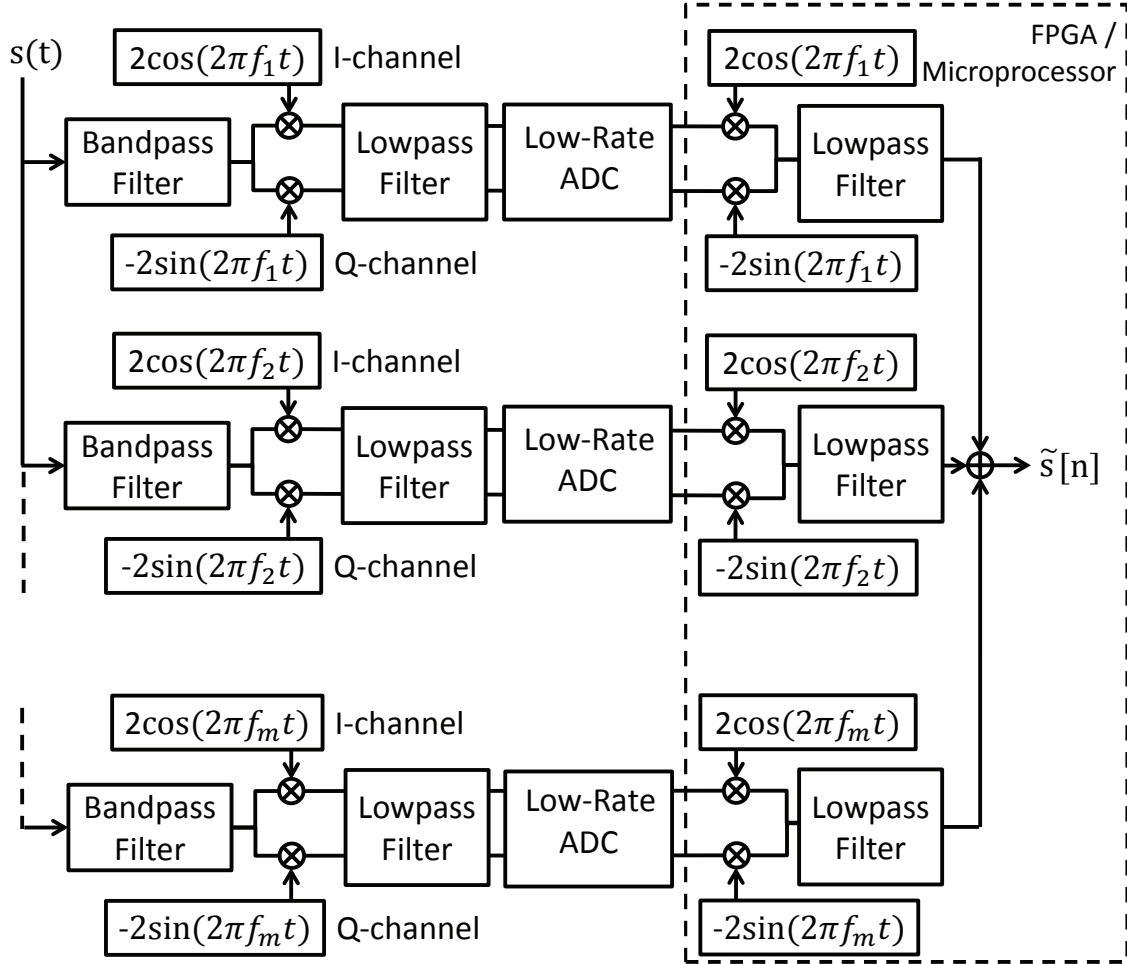


Figure 2.3. Multiple Low-Rate Samplers (MLRS) Receiver

THIS PAGE INTENTIONALLY LEFT BLANK

CHAPTER 3:

Recovery and Detection Theory

3.1 Signal Recovery Error

The first point of interest is how much similarity there is between the recovered and original signal. The metric used is the sum-squared error (SSE) which is given by

$$J = \frac{\sum_{n=0}^{N-1} |x[n] - \tilde{s}[n]|^2}{E}, \quad (3.1)$$

where $x[n]$ is the original signal, $\tilde{s}[n]$ is the recovered signal (where noise is present), and E is the energy of $x[n]$. We have expanded upon the SSE in [6] by normalizing the SSE by E .

Once again observe the signal-plus-noise magnitude spectrum in the top panel of Figure 3.1. After applying our MLRS technique, the magnitude spectrum is shown in the bottom panel of Figure 3.1. Notice that our MLRS technique does not exactly recover (or reconstruct) the signal completely. The non-dominant amplitudes are attenuated. Clearly, some signal energy or information is lost. Notice also that the noise in these bands is attenuated; thus, two questions arise. First, will the attenuation in signal increase the SSE of MLRS or the attenuation of noise actually lower the SSE? Second, how is the detection probability affected knowing that potentially a large portion of signal energy is removed by the MLRS filters?

3.2 Matched Filters

The detection performances of the MLRS and traditional high-rate sampling receiver, each with its own respective matched filter, are compared in this work. A matched filter is proven to maximize the SNR when a signal is present in white Gaussian noise. The complete derivation of a matched filter for a known signal is shown in [7]. Here, only the results are summarized, and the notation is updated to reflect our work. The optimal filter for the signal $x(t)$ is given by

$$h(t) = kx^*(\tau - t), \quad (3.2)$$

where k is an arbitrary gain, τ is the duration of the signal, and $*$ represents the conjugate operation.

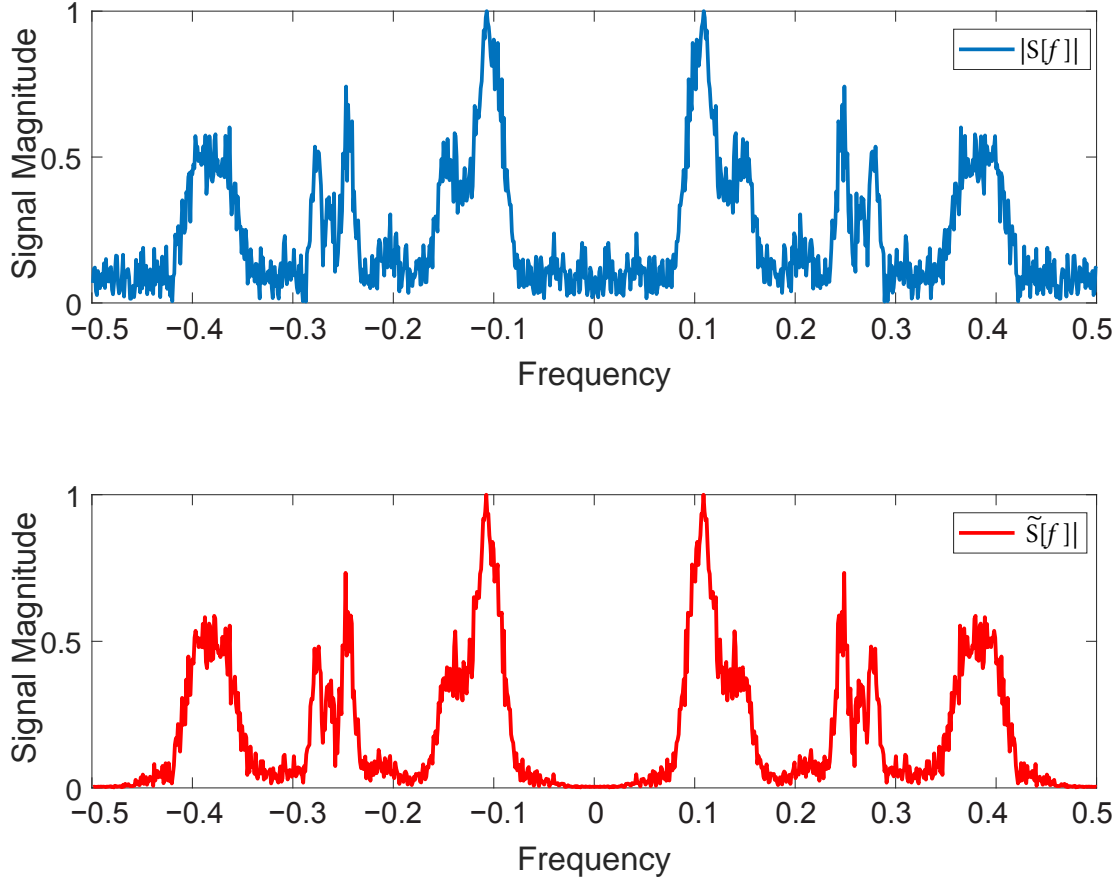


Figure 3.1. Test Signal in Noise Spectrum (top) and its Corresponding Reconstruction Spectrum (bottom)

3.3 Probability of Detection — Matched Filter

We wish to compare the probability of detection P_D using our proposed MLRS design vice the signal's broadband matched filter used in a traditional high-rate sampling receiver. In matched filter receiver design, a given probability of false alarm P_{FA} specification gives

rise to the receiver threshold

$$\gamma' = \sqrt{\sigma^2 E} Q^{-1}(P_{FA}), \quad (3.3)$$

where σ^2 is the sample variance of the white Gaussian noise, E is the energy of the real signal $x[n]$, and Q^{-1} represents the inverse Q-function [8]. It can be shown that the P_D for a specified signal-to-noise ratio E/σ^2 and P_{FA} is given by

$$P_D = Q\left(Q^{-1}(P_{FA}) - \sqrt{\frac{E}{\sigma^2}}\right). \quad (3.4)$$

It is clear from (3.4) that as the SNR increases so does P_D . Additionally, the P_D is independent of the signal's shape. The theoretical P_D curve for a signal with $P_{FA} = 10^{-2}$ is shown in Figure 3.2.

3.4 Probability of Detection — MLRS

The matched filter P_D can be generalized and applied to the MLRS receiver. It has been made clear that the signal energy and noise are reduced by the receiver. The recovered signal energy and noise variance can be determined mathematically or via simulation. An important effect that must now be accounted for is the filtering of the white Gaussian noise. This noise is no longer uncorrelated but has some defined covariance \mathbf{C} and must be included in the P_D derivation. The P_D for the MLRS receiver is given by

$$P_D = Q\left(Q^{-1}(P_{FA}) - \sqrt{\tilde{\mathbf{x}}' \mathbf{C}^{-1} \tilde{\mathbf{x}}}\right), \quad (3.5)$$

where $\tilde{\mathbf{x}}$ is the noise-free reconstruction of \mathbf{x} , \mathbf{C} is the noise covariance matrix due to the MLRS filters, and $'$ represents the transpose operation [8]. With a known or accurate estimate of the covariance matrix of the noise, the P_D given by (3.5) matches the P_D given by (3.4).

3.5 Monte Carlo Simulation

While it can be shown theoretically that the P_D for the MLRS receiver is given by (3.5), we determine the P_D of the MLRS receiver through a Monte Carlo simulation. We wish to find the P_D via determining the number of times the decision statistic is greater than the

threshold. The decision statistic T is given by

$$T(\tilde{s}) = \tilde{\mathbf{x}}' \mathbf{C}^{-1} \tilde{s}, \quad (3.6)$$

where $\tilde{s}[n]$ is the recovered signal with noise present.

The threshold γ' is given by

$$\gamma' = \sqrt{\tilde{\mathbf{x}}' \mathbf{C}^{-1} \tilde{\mathbf{x}}} Q^{-1}(P_{FA}). \quad (3.7)$$

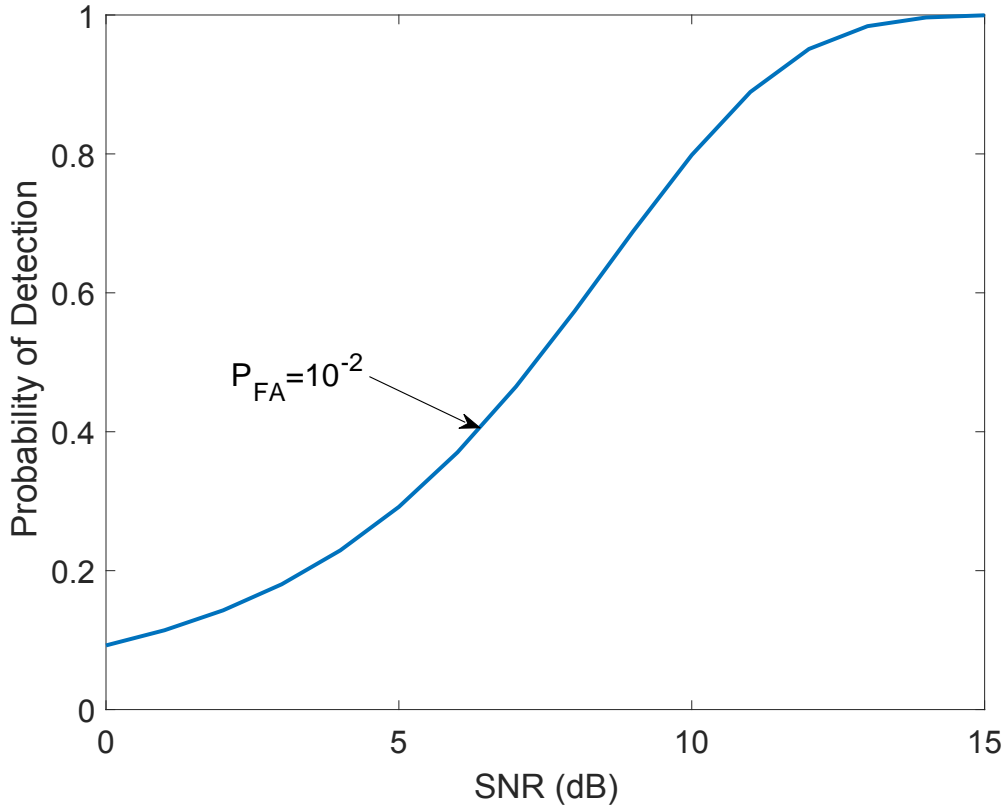


Figure 3.2. Theoretical Matched Filter Detection Performance for a $P_{FA} = 10^{-2}$

The signal flow diagram is shown in Figure 3.3 to indicate the signal variables and the detection process. The signal is considered present if the detection statistic exceeds the threshold; thus P_D is found by dividing the number of times the threshold is exceeded by

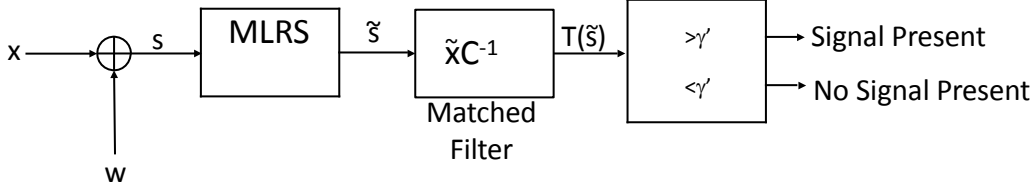


Figure 3.3. Signal Detection Flowpath

the number of trials. This process is repeated across a range of SNR values. The number of Monte Carlo trials at a given SNR throughout this work is 5,000.

The SNR is adjusted by increasing the signal energy as opposed to changing the noise variance. We let the sample variance of the noise equal unity in this work. In the development of test signal $x[n]$, we emphasized the shape and relative scale of the peaks in the frequency response and not necessarily the signal energy. This must now be corrected to achieve the correct SNR. First, the signal energy is normalized. Next, $x[n]$ is multiplied by a gain $k = \sqrt{SNR}$, where SNR is in its decimal form.

3.6 Recovered Signal

Both the signal and noise energy are reduced by the MLRS receiver, although not equally. Energy outside of the selected bands is greatly attenuated, while these dominant bands are filtered into subchains for processing.

3.6.1 Signal Energy

The receiver clearly reduces the signal energy in the non-dominant portions of the spectrum. The exact amount is dependent upon the signal and receiver design. Aspects of receiver design include the number of subchains and the parameters associated with filter design.

The noise-free test signal and its reconstruction are compared in the Figure 3.4. Visually, the reconstruction $\tilde{x}[n]$ appears to be a good representation of the original signal $x[n]$. The sum-squared error quantifies how closely the recovered signal is to the original.

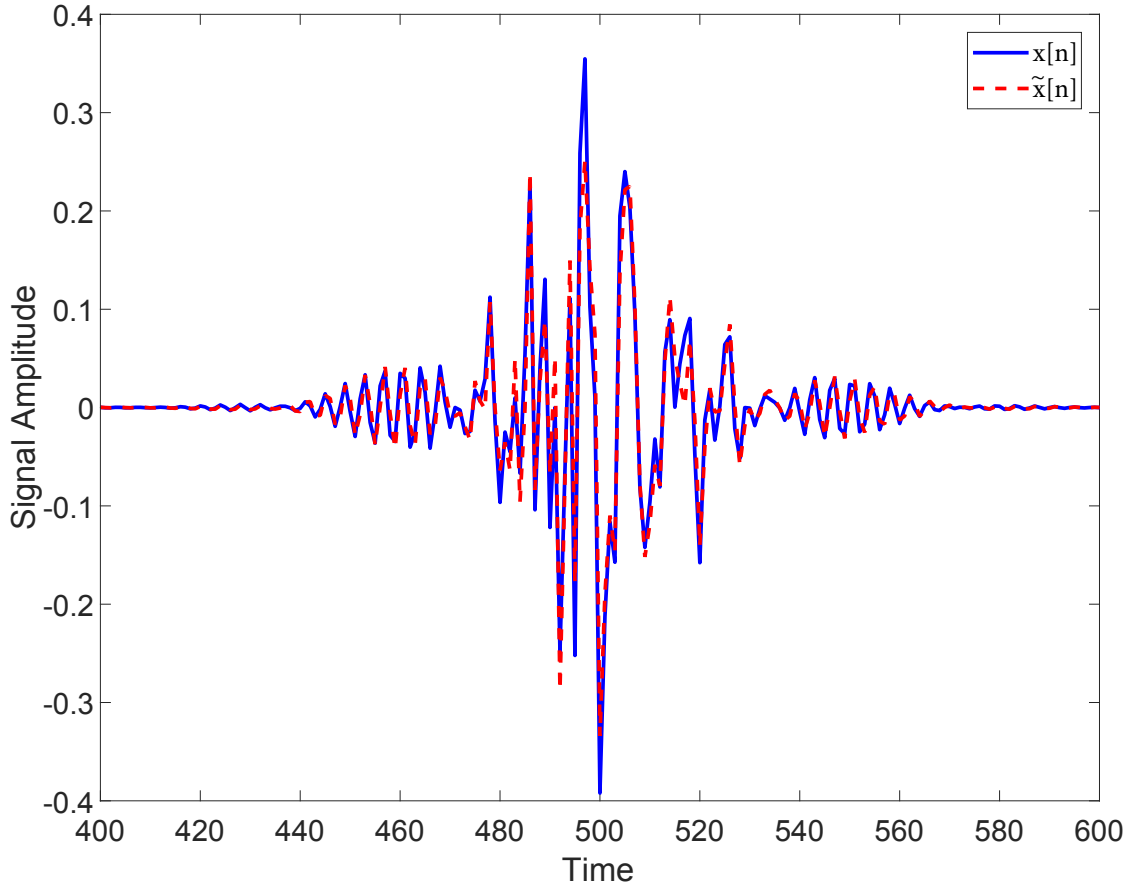


Figure 3.4. Noise-Free Test Signal and its MLRS Reconstruction

3.6.2 Noise in the Frequency Domain

It is interesting to see what happens to the noise when going through the MLRS filters. In the top panel of Figure 3.5 the Fourier transform of a white Gaussian noise realization is shown. In the bottom panel, another Fourier transform of a white Gaussian noise realization is shown after MLRS receiver processing. The noise is now altered by the selective filtering at the specified bands. Notice the attenuation effects of the three MLRS filters. While the noise vector is no longer uncorrelated, it still follows a Gaussian distribution but with a certain covariance matrix. The noise covariance is accounted for in the matched filter; therefore, the detection performance depends upon the covariance of the noise.

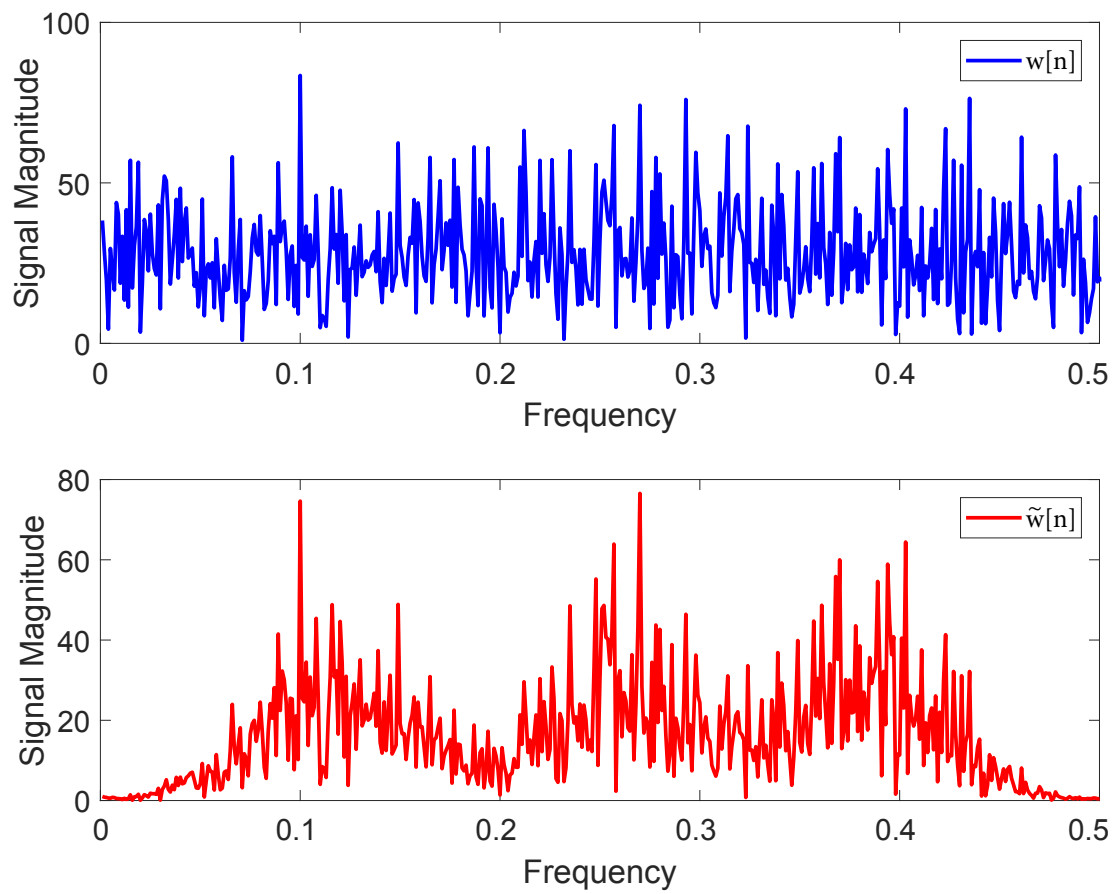


Figure 3.5. White Gaussian Noise Spectrum (top) and its MLRS Reconstruction Spectrum (bottom)

THIS PAGE INTENTIONALLY LEFT BLANK

CHAPTER 4:

Test Signal Results

The results from calculation, simulation, and hardware implementation for the test signal are presented here. Recall that the signal is arbitrarily designed but is representative of wideband yet not-so-sparse time-domain signals that MLRS is supposed to address.

4.1 Simulation Configuration Parameters

In order to quantify and better understand the following results, the receiver filter design specifications are listed in Table 4.1. Recall in Figure 2.2 that the signal has three dominant portions in the spectrum; thus, three subchains are designed for the receiver. Finite-impulse response (FIR) filters are used in the MLRS receiver subchains.

Table 4.1. Model Design Parameters for Test Signal

Filter	Order	Passband
Bandpass 1	20	0.0665-0.1815
Bandpass 2	20	0.2295-0.2935
Bandpass 3	20	0.3225-0.4415
Lowpass	20	0-0.09

Low-order filters are chosen to keep the computational complexity and cost low. The combination of filter order and passband resulted in approximately 60% of the spectrum bandwidth being rejected by this receiver design, but 82% of the signal energy was retained.

4.2 Sum-Squared Error

We look first at the reconstruction of the signal using MLRS. It is shown that the dominant bands of the original signal are not attenuated as are the amplitudes outside these bands in Figure 3.1. While the attenuation may be disconcerting since it does reduce the signal energy and affect reconstruction, the MLRS effectively reduces the noise power more than it reduces the signal power. The SSE decreases with increasing SNR for both MLRS and traditional high-rate sampling receivers as seen in Figure 4.1. It is clear that MLRS

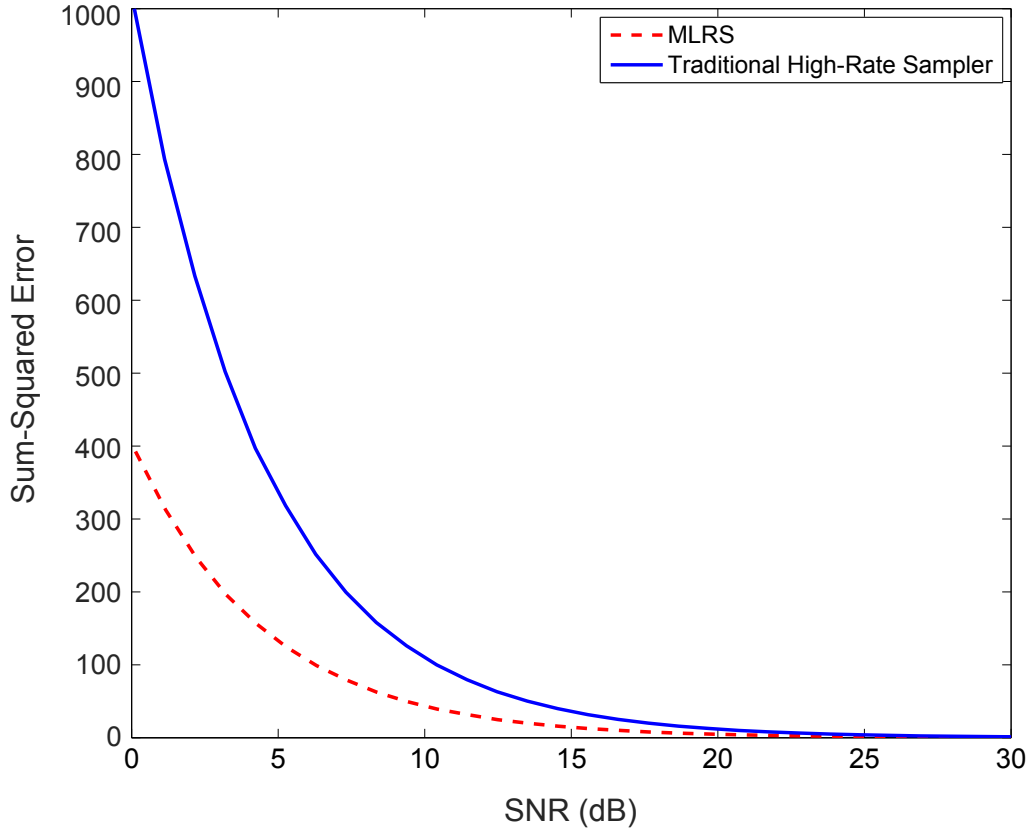


Figure 4.1. MLRS and Traditional High-Rate Sampler Sum-Squared Error for Test Signal

improves the SSE. The MLRS provides a more accurate representation of the original by selectively filtering the signal when compared to the output of the signal sampled by a traditional high-rate sampler.

Due to our definition of the SSE, a second observation can be made about the SSE. The SSE is defined as the summed difference between the signal and its reconstruction (or signal plus some noise in the case of the traditional high-rate sampler) squared. For the traditional high-rate sampler, once the signal plus some noise is subtracted from the signal, we are left only with the noise. This simplified relation is given by

$$J = \frac{\sum_{n=0}^{N-1} |w[n]|^2}{\sigma^2 SNR}, \quad (4.1)$$

where the test signal energy E is replaced by $\sigma^2 SNR$. We can simplify this further since the SNR at 0 dB is 1.0; and the SSE is 1,000 at 0 dB. Rearranging this equation for σ^2 gives

$$\sigma^2 = \frac{\sum_{n=0}^{N-1} |w[n]|^2}{1000}. \quad (4.2)$$

Noise generation in Matlab shows the numerator of this equation approaches 1,000; therefore, $\sigma^2 = 1.0$, which is the sample noise variance used for our simulations. Similarly this explanation can be applied to the MLRS. In this case, the difference between the signal and its reconstruction does not perfectly cancel out the test signal to result in only noise; however, the MLRS filters attenuate the noise more than the signal, and thus, the noise variance is lowered, which in turn lowers the SSE. The effective noise variance is approximately 0.428 for the MLRS receiver. When the SNR is increased in Figure 4.1, the signal energy is increased while keeping the noise variance as unity; thus, the increasing signal energy causes the SSE to decrease.

4.3 Probability of Detection Results

Next we analyze the effect of MLRS on probability of detection. As noise is attenuated and the signal's dominant bands are retained, we anticipate that P_D is not degraded significantly as long as the estimate of the noise covariance is accurate. The P_D for various P_{FA} are shown in Figure 4.2. For each given P_{FA} , the MLRS receiver agrees well with the performance of the traditional wideband matched filter. Here we recall that the MLRS matched filter includes the noise covariance matrix. In our work, the covariance matrix is determined via simulation. These results are generated via MATLAB script and confirmed by a Simulink model. It should be noted that a second probability of detection scenario was conducted without inclusion of the covariance matrix. The threshold was tuned to achieve the correct P_{FA} , but this resulted in poorer detection performance. This is because the resulting noise due to the FIR filters is now correlated; thus, to achieve the original detection curve for the test signal, the covariance matrix is needed to whiten the noise output of the MLRS matched filter.

Despite the detection performance and gains on SSE, we note that one of the more exciting advantages of this work is the use of low-rate samplers. It is well known that a single high-rate ADC is more expensive than an integrated chip (IC) containing low-rate ADCs.

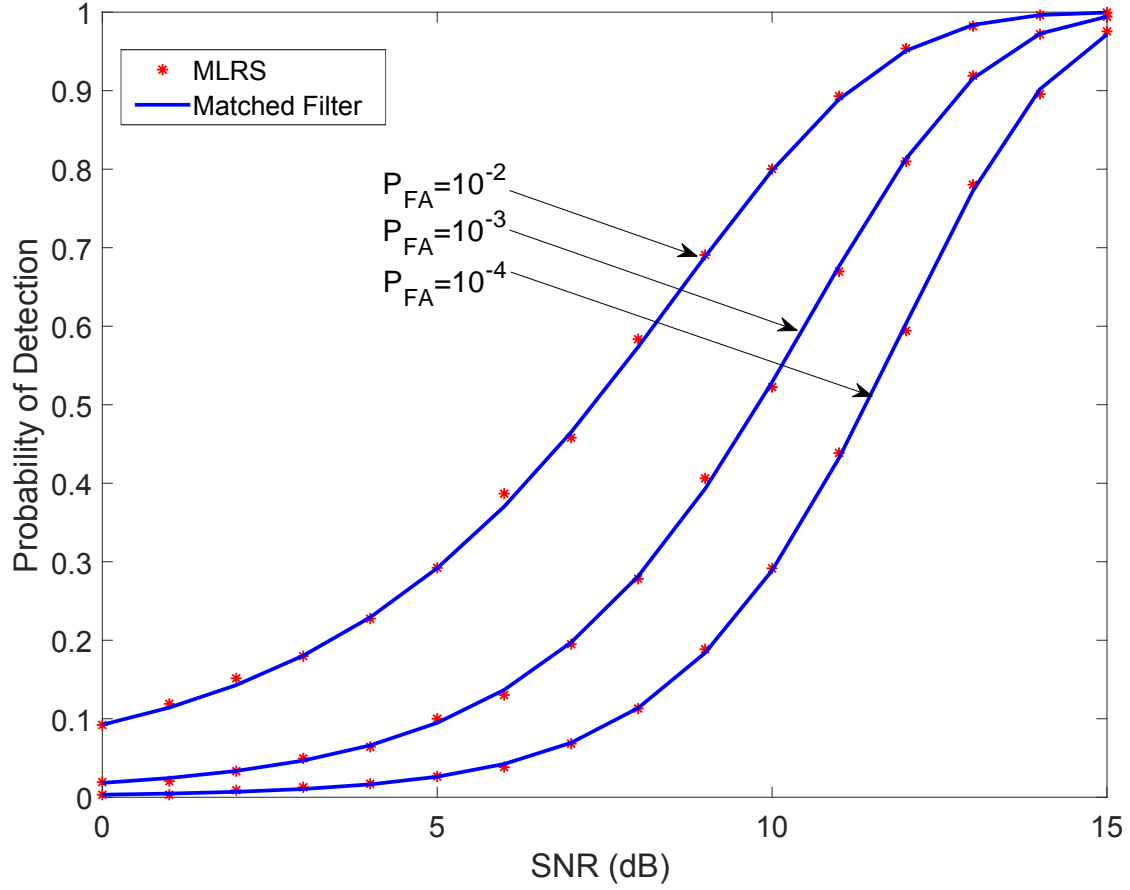


Figure 4.2. MLRS and Matched Filter Detection Performance for Test Signal for $P_{FA} = 10^{-2}$, 10^{-3} , and 10^{-4}

For example, a 1.0 Gbps ADC costs on the order of a few hundred dollars, whereas an identical ADC in terms of bit precision (number of quantization bits) with a 10.0 Mbps rate costs less than ten dollars [9],[10].

In practice, low-cost integrated chip packages of two or four ADCs are readily available. By using these low-rate samplers, both actual cost and computational cost are significantly reduced. Each receiver subchain can be sampled individually at a reduced rate of F_s/D_i without any degradation in the probability of detection. For the particular signal in Figure 2.2, the corresponding D_i s for each $\psi_i[f]$ are $D_1 = 4$, $D_2 = 7$, and $D_3 = 4$. The probability of detection is shown using these D_i in Figure 4.2.

4.4 Hardware Modeling

The Simulink and MATLAB simulation models are identical in terms of results up until this point as they both use double-precision arithmetic and are primarily mathematical models in each case. In order to physically realize this model on an FPGA, the Simulink model was converted to fixed-point precision, and basic arithmetic blocks were replaced with hardware description language (HDL) optimized blocks. These blocks are required to generate the C and HDL to program the processor and FPGA for operations. The Xilinx synthesis tool was used to create the bitstream and once generated, this bitstream was downloaded to the local secure digital (SD) card on the FPGA. This programming method allows the board to restart without loss of the programmed data.

The resulting Simulink model which was implemented in hardware is detailed in Figure 4.3. Note that only a single receiver subchain is shown. In reality there are three channels for the test signal. The overall design is similar to that described in Figure 2.3. One exception is that the entire process is digital, and the complete MLRS receiver architecture is modeled on the FPGA rather than what is indicated inside the dashed box in Figure 2.3.

The HDL workflow advisor in Simulink compiles C and HDL programming language to execute functions on the processor and FPGA, respectively. In addition, a model interface is generated which loosely resembles the original Simulink model. In this representation the filters, oscillators, and various receiver components are written in C or VHDL, and the model simply connects our inputs from the model workspace to the board through an AXI-Lite interface. In the same way, the output of the board is fed through an AXI-Lite interface back into the workspace.

The Xilinx Zynq-7000 SoC ZC706 is chosen for our hardware implementation of the MLRS receiver. This board and the connections used are shown in Figure 4.4. The UART connection on the board is used to create a serial connection using PuTTY to monitor the onboard performance and conduct diagnostics. The Ethernet connection is used for data transfer between the board and Simulink workspace. The board is controlled through a Matlab script which initiates the Simulink graphic model interface linked to the MLRS program downloaded on the FPGA SD card.

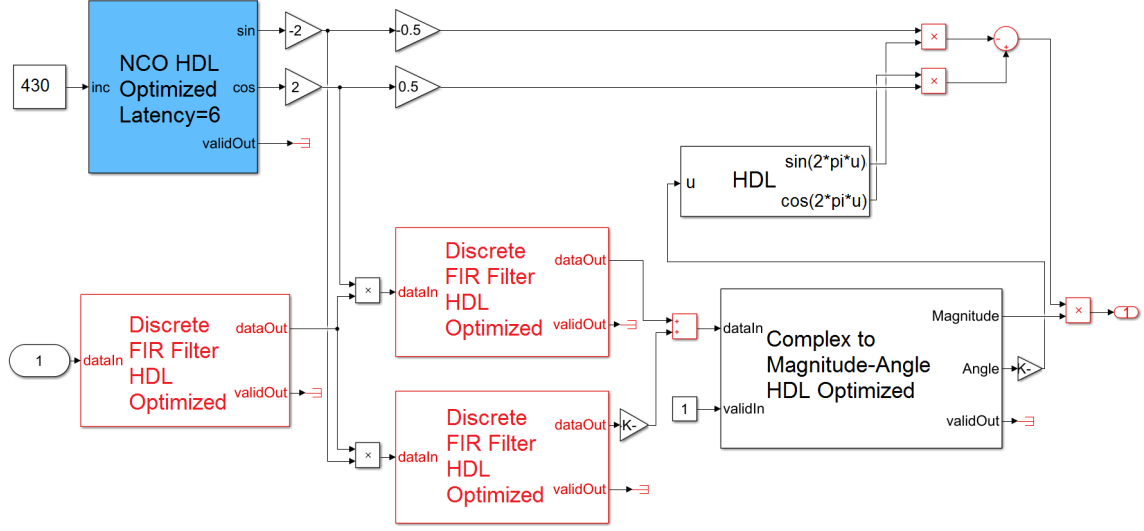


Figure 4.3. Simulink Receiver Subchain Model

4.5 Hardware Results

Probability of detection results from the hardware are expected to match the performance shown by the MATLAB and Simulink simulation models with some small variations depending on the number of Monte Carlo trials used. The inclusion of hardware is an important proof-of-concept in the process of fielding this technology. The successful programming of the hardware demonstrates the ability of the receiver to operate without external intervention.

The hardware detection performance is shown alongside the previous simulation results in Figure 4.5. The hardware results are consistent with the previous simulations. The slight P_D degradation in the hardware results is likely from quantization, estimation of the noise covariance, and fixed-point precision. Graphically shown here are the results from setting the P_{FA} to 10^{-2} , but similar results are found across the range of false alarm probabilities. Again, meeting the detection performance of a matched filter is an important check, but the benefit of this work comes from the low-rate ADCS. Here the individual channels are sampled at the reduced rate of F_s/D_i , and the corresponding D_i s for each $\psi_i[f]$ are $D_1 = 4$, $D_2 = 7$, and $D_3 = 4$.

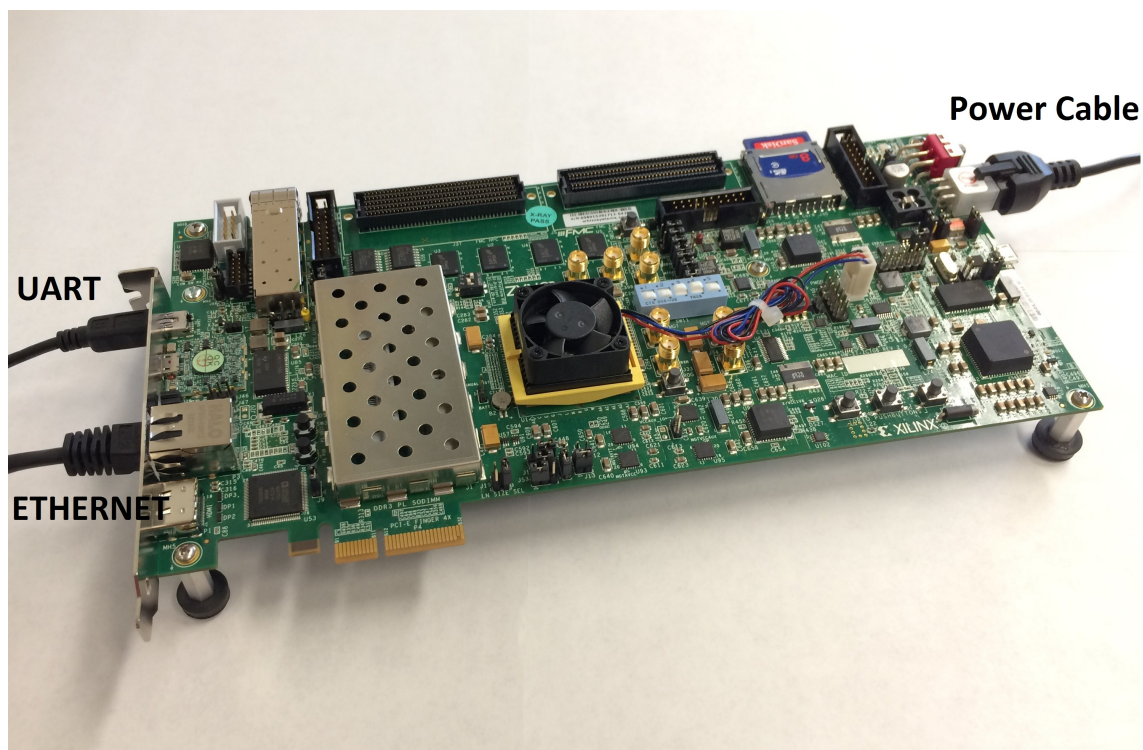


Figure 4.4. Xilinx Zynq-7000 SoC ZC706

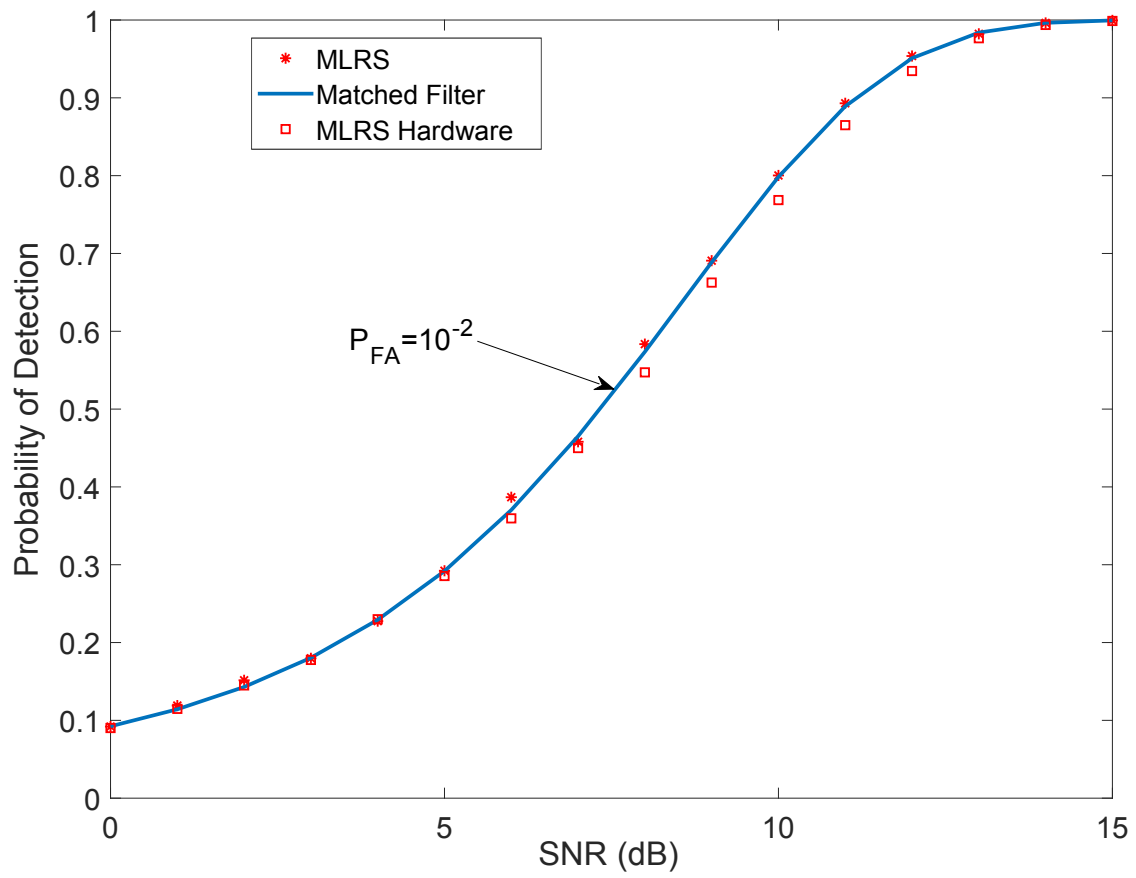


Figure 4.5. MLRS Hardware Detection Performance for Test Signal for $P_{FA} = 10^{-2}$

CHAPTER 5:

Practical Target Model and Results

In this chapter a practical target response is considered. Here, we use a radar cross section (RCS) frequency response generated from an electromagnetic software simulation. The same performance metrics of sum-squared error and probability of detection are tested in Matlab, Simulink, and hardware. Observations between the real signal and example signal of the previous section are made.

5.1 RCS Target Response

Now that the MLRS concept has been proven successful for the initial test signal, we wish to apply the MLRS to a practical signal and investigate the improvement in SSE and its effect on detection probability. The signal chosen is a particular frequency response from an A6 tank [11]. The physical target and the frequency response are shown in Figure 5.1. This target response uniquely corresponds to the aspect angle of $\phi = 0^\circ$ and $\theta = 45^\circ$. Apart from being a RCS target response, the signal is at a higher frequency band than the previously modeled signal. The A6 signal is measured from 3-4 GHz. In simulation the sampling time is normalized.

Unlike the previous signal, the dominant bands in the A6 signal are less clear. Seven prominent $\psi_i[f]$ are chosen for the MLRS receiver design. They are shown in Figure 5.1. We briefly considered an alternate design using five subchains. In this model $\psi_4[f]$, $\psi_5[f]$, and $\psi_6[f]$ were combined together under a single center frequency. The preliminary P_D results from this variant were the same of those of the seven channel design. Recall that the combining of multiple resonant amplitudes under a single center frequency was also performed with the test signal in Figure 2.2.

5.2 Simulation Configuration Parameters

The receiver for the real target signal is architecturally the same as that for the previous signal but differs in the number of subchannels and filter parameters. The receiver design

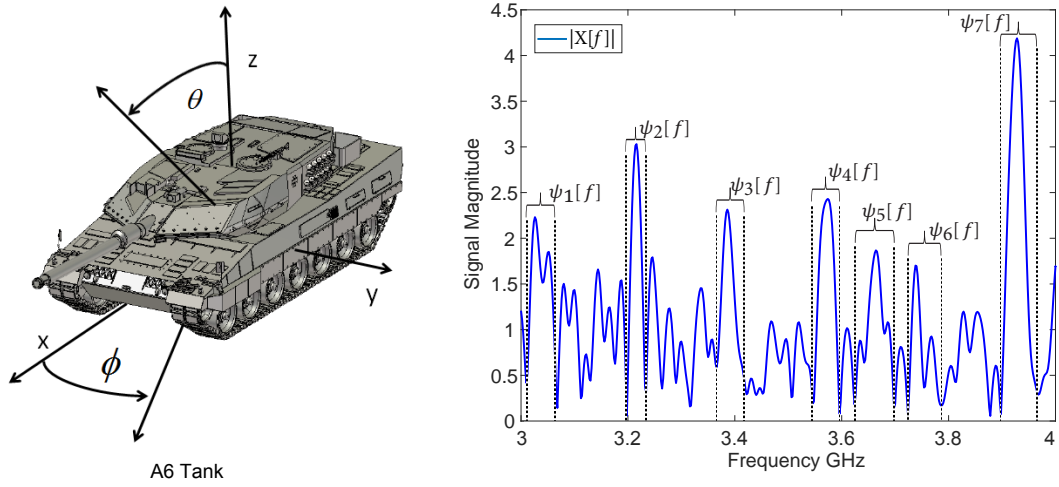


Figure 5.1. A6 Tank Model and Frequency Response for $\phi = 0^\circ$ and $\theta = 45^\circ$. Adapted from [11].

specifications are listed in Table 5.1. As shown in Figure 5.1, the signal has seven dominant portions in the spectrum; thus, seven subchains are designed for the receiver.

Table 5.1. Model Design Parameters for A6 Signal

Filter	Order	Passband
Bandpass 1	80	0.0075-0.0225
Bandpass 2	80	0.1075-0.1085
Bandpass 3	80	0.185-0.210
Bandpass 4	80	0.275-0.295
Bandpass 5	80	0.322-0.349
Bandpass 6	80	0.369-0.371
Bandpass 7	80	0.455-0.475
Lowpass	80	0-0.125

Apart from the changes in the passband of the filters, the order of the bandpass filters is also increased. Higher order filters are chosen to allow a steeper roll-off between the passband and stopband. This allows for finer selection of the bands and better reconstruction of the signal. Higher order filters generally increase the number of computations but not significantly in this case.

In addition to the desire to have better control over the passband and stopband, higher order filters are chosen to reject more of the noise and prevent filter overlap. Due to the number of channels and their spacing, if low-order filters are used, the filters overlap. While overlapping filters is not necessarily a problem, it is not the approach we are proposing for our receiver design. In this MLRS design approximately 78% of the spectrum bandwidth is rejected by this MLRS design but 57.6% of the signal energy is retained.

The order of lowpass filters could remain at 20 for specific channels. In most subchains the gap in the spectrum between the desired baseband signal and the intermodulation products is large; thus, a lower-order filter is adequate. There are two particular subchains in which we are not able to use low-order filters. These filters do not adequately attenuate the intermodulation products within these two subchains and cause distortion in the reconstruction. In order to keep filter order uniform, higher-order filters are chosen for all subchains.

5.3 Sum-Squared Error

We begin by comparing the similarity between the reconstructed signal and the original. The baseline for our comparison is the output signal of the traditional high-rate sampling receiver. The results are displayed in Figure 5.2. The MLRS receiver is shown to have better SSE than the traditional wideband receiver. The effective variance of the noise at the output of the MLRS is shown to be 0.21 at a SNR of 0 dB.

5.4 Probability of Detection

In the probability of detection scenario we once again compare the MLRS receiver against a traditional wideband matched filter. The setup and simulation procedure used for the previous signal is unchanged. The results from both the Matlab and Simulink simulations are shown in the top panel of Figure 5.3. Each channel was sampled at a reduced rate of F_s/D_i without any degradation in the probability of detection. The D_i is found for each channel from (2.2). The D_i s for each $\psi_i[f]$ are $D_1 = 16$, $D_2 = 25$, $D_3 = 10$, $D_4 = 12$, $D_5 = 9$, $D_6 = 25$, and $D_7 = 12$. Not all of the channels here are sampled at the minimum sampling rate. Theoretically, $\psi_2[f]$ and $\psi_6[f]$ have a higher D_i due to the very narrow bandwidth occupied by these resonant portions of the spectrum, but this is impractical in a digital simulation. The higher D_i results in discarding too much of the signal for

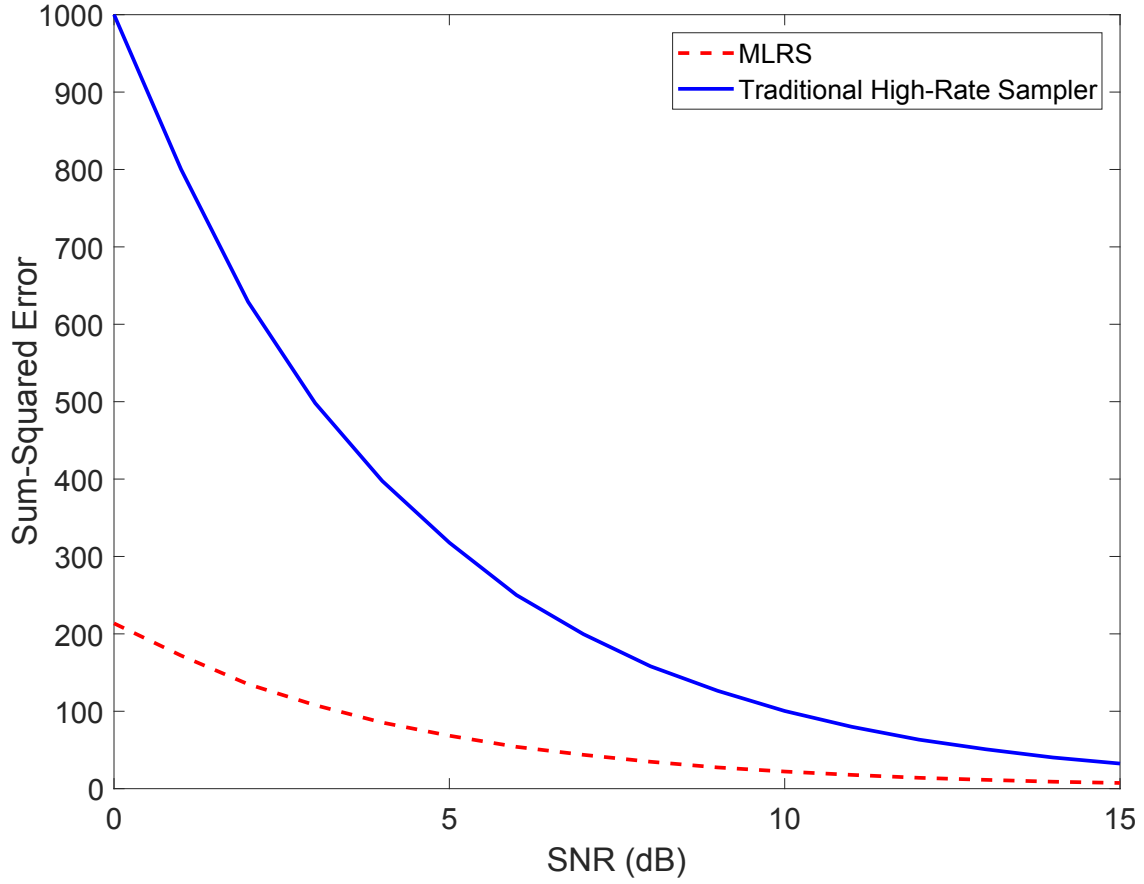


Figure 5.2. MLRS and Traditional High-Rate Sampler Sum-Squared Error for A6 Target Response

reconstruction. These two dominant portions are represented by only a few samples, and it is possible to completely skip the narrow peaks with a higher D_i . Thus, a smaller, yet substantial value is chosen for D_2 and D_6 .

The P_D results graphically look very similar to that produced for the example signal. The Matlab and Simulink simulation models both follow the detection performance of the matched filter closely. The hardware results are shown in the bottom panel of Figure 5.3. There is a slight degradation due to quantization and covariance estimation, but the performance is still comparable to that of a matched filter.

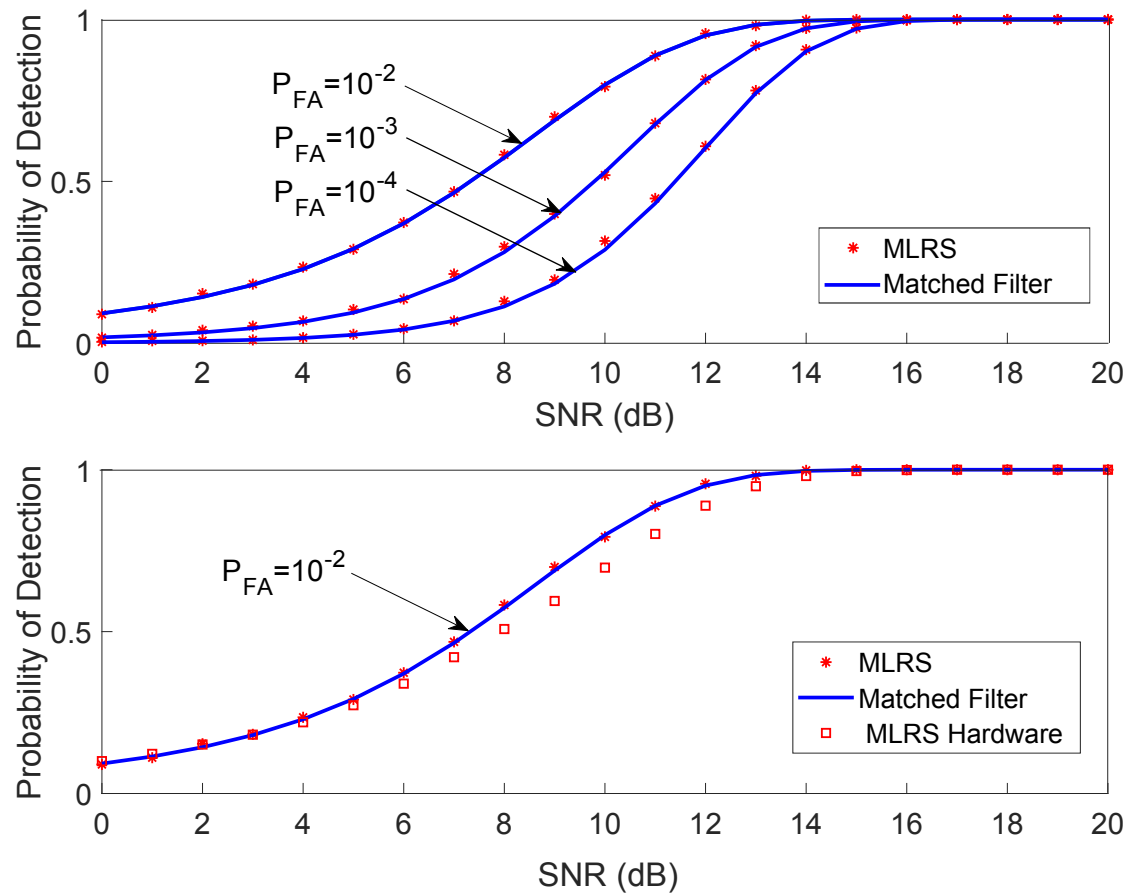


Figure 5.3. MLRS and Matched Filter Detection Performance (top) and MLRS Hardware Detection Performance (bottom) for A6 Target Response

THIS PAGE INTENTIONALLY LEFT BLANK

CHAPTER 6:

Conclusion

6.1 Summary of Results

In this study it has been shown that particular wideband signals with dominant amplitudes at specific frequency bands can be sampled at a lower total effective sampling rate. The method has been shown to be applicable to both arbitrary and practical target signals. The MLRS technique solves the requirement of a high sampling rate and retains the signal's probability of detection. It was shown that the MLRS performed as well as a traditional high-rate sampler with a matched filter in Matlab and Simulink simulation models. Hardware results indicated a slight degradation in performance of the MLRS probability of detection compared to the theoretical performance. In addition, it was shown that the MLRS improved the reconstruction of the signal. The sum-squared error was less for the MLRS because the effective noise variance was lowered.

6.2 Future Work

While the signal was tested on hardware, there is still significant work to be explored in this area. The concept was proven to run alone on the board while a signal was sent from the computer to the board and back. In future simulations and in practical applications, the signal must be received over the air. The framework for this is already in place, and the hardware is readily available.

While the method was shown to be successful, the methodology for selecting the resonant frequency bands was based on arbitrarily choosing the bandwidths of the subbands. In other words, practical guidelines can be developed when choosing the center frequencies and the subband energies to be preserved by the filters. The filter order was chosen to be small. The FIR filters were chosen for simplicity. A trade-off study between different types of filters would benefit this research.

The exact covariance structure of the noise can be mathematically determined but was not the focus of our work. Derivation of the exact noise covariance after the summation of filter

outputs would save time and add value to the hardware's adaptability.

List of References

- [1] D. L. Donoho, “Compressed sensing,” *IEEE Trans. Inf. Theory*, vol. 52, no. 4, pp. 1289-1306, Apr., 2006.
- [2] E. J. Candes, J. Romberg and T. Tao, “Robust uncertainty principles: Exact signal reconstruction from highly incomplete frequency information,” *IEEE Trans. Inf. Theory*, vol. 52, no. 2, pp. 489-509, Feb., 2006.
- [3] R. G. Baraniuk, “Compressive sensing [lecture notes],” *IEEE Trans. Signal Process.*, vol. 24, no. 4, pp. 118-121, Jul., 2007.
- [4] G. L. Fudge, R. E. Bland, M. A. Chivers, S. Ravindran, J. Haupt and P. E. Pace, “A Nyquist folding analog-to-information receiver,” 2008 42nd Asilomar Conference on Signals, Systems and Computers, Pacific Grove, CA, 2008, pp. 541-545. [Online]. doi: 10.1109/ACSSC.2008.5074464
- [5] F. Harris, E. Venosa, X. Chen and C. Dick, “Interleaving different bandwidth narrowband channels in perfect reconstruction cascade polyphase filter banks for efficient flexible variable bandwidth filters in wideband digital transceivers,” 2015 IEEE International Conference on Digital Signal Processing (DSP), Singapore, 2015, pp. 1111-1116. [Online]. doi: 10.1109/ICDSP.2015.7252051
- [6] N. R. Draper, *Applied Regression Analysis*, 3rd ed. Hoboken, NJ, USA: John Wiley and Sons, Inc., 1998.
- [7] B. R. Mahafza, *Radar Systems Analysis and Design Using MATLAB*, 2nd ed. Boca Raton, FL, USA: Chapman and Hall/CRC, 2005.
- [8] S. M. Kay, *Fundamentals of Statistical Signal Processing, Volume I: Estimation Theory*. Upper Saddle River, NJ: Prentice Hall, 1993.
- [9] Analog Devices, “AD9234 (Rev. B),” AD9234 datasheet, Aug. 2014 [Revised Jan. 2018]. [Online]. Available: <http://www.analog.com/media/en/technical-documentation/data-sheets/ad9234.pdf>

- [10] Analog Devices, “TC2225,” LTC2225 datasheet, 2004 [Rev A]. [Online]. Available: <http://www.analog.com/media/en/technical-documentation/data-sheets/2225fa.pdf>
- [11] Q. J. O. Tan, R. A. Romero and D. C. Jenn, “Target recognition with adaptive waveforms in cognitive radar using practical target RCS responses,” 2018 IEEE Radar Conference (RadarConf18), Oklahoma City, OK, 2018, pp. 0606-0611. [Online]. doi: 10.1109/RADAR.2018.8378628

Initial Distribution List

1. Defense Technical Information Center
Ft. Belvoir, Virginia
2. Dudley Knox Library
Naval Postgraduate School
Monterey, California